Graham Feld
Shell Projects & Technology,
Aberdeen AB12 3FY, UK
e-mail: graham.feld@shell.com

David Randell
Shell Projects & Technology,
Manchester M22 0RR, UK
e-mail: david.randell@shell.com

Yanyun Wu
Shell Projects & Technology,
Manchester M22 0RR, UK
e-mail: yanyun.wu@shell.com

Kevin Ewans
Sarawak Shell Bhd,
Kuala Lumpur 50450, Malaysia
e-mail: kevin.ewans@shell.com

Philip Jonathan
Shell Projects & Technology,
Manchester M22 0RR, UK
e-mail: philip.jonathan@shell.com

Estimation of Storm Peak and Intrastorm Directional–Seasonal Design Conditions in the North Sea

Specification of realistic environmental design conditions for marine structures is of fundamental importance to their reliability over time. Design conditions for extreme waves and storm severities are typically estimated by extreme value analysis of time series of measured or hindcast significant wave height, H_S. This analysis is complicated by two effects. First, H_S exhibits temporal dependence. Second, the characteristics of H_S^{sp} are nonstationary with respect to multiple covariates, particularly wave direction, and season. We develop directional–seasonal design values for storm peak significant wave height (H_S^{sp}) by estimation of, and simulation under a nonstationary extreme value model for H_S^{sp}. Design values for significant wave height (H_S) are estimated by simulating storm trajectories of H_S consistent with the simulated storm peak events. Design distributions for individual maximum wave height (H_{max}) are estimated by marginalization using the known conditional distribution for H_{max} given H_S. Particular attention is paid to the assessment of model bias and quantification of model parameter and design value uncertainty using bootstrap resampling. We also outline existing work on extension to estimation of maximum crest elevation and total extreme water level.
[DOI: 10.1115/1.4029639]

1 Introduction

Specification of realistic environmental design conditions for marine structures is of fundamental importance to their reliability over time. Design conditions for extreme waves and storm severities are typically estimated by extreme value analysis of time series of measured or hindcast significant wave height, H_S. This analysis is complicated by two effects.

First, H_S exhibits temporal dependence, invalidating naive application of extreme value analysis. Instead, time series must be declustered into observations of (independent) storm peak significant wave height H_S^{sp}, and (intrastorm) directional dissipation of H_S conditional on H_S^{sp}. Extreme value analysis is then performed on H_S^{sp} providing a mechanism to simulate storm peak events for arbitrary return periods. Design values for H_S (for an arbitrary storm sea-state) are next estimated by incorporation of dissipation effects within the simulation. Design distributions for individual maximum wave height H_{max} can then be estimated by marginalization using the known conditional distribution for H_{max} given H_S. Design values for other intrastorm variables such as maximum crest elevation and total extreme water level can be estimated similarly.

Second, the characteristics of H_S^{sp} are nonstationary with respect to multiple covariates, particularly wave direction and season. Failure to accommodate nonstationarity can lead to incorrect estimation of design values. As shown in OMAE2013-10187, covariate effects in peaks over threshold of H_S^{sp} can be modeled in terms of nonstationary models for extreme value threshold (using quantile regression model), the rate of occurrence of threshold exceedances (using a Poisson model), and the sizes of exceedances (using a generalized Pareto (GP) model). Model parameters are described as smooth functions of covariates using appropriate multidimensional penalized B-splines. Optimal parameter smoothness is estimated using cross-validation.

In this work, we develop directional–seasonal design values for H_S^{sp}, H_S, and H_{max} for a location in the North Sea. Particular attention is paid to the assessment of model bias and quantification of model parameter and design value uncertainty using bootstrap resampling. We also outline existing work on extension to estimation of maximum crest elevation and total extreme water level.

The use of design criteria varying with direction is well-established, particularly for in-place reassessments and reliability studies of fixed jacket structures. However, there are certain situations where design criteria varying with both season and direction may be more appropriate. One example is site-specific assessments of jack-up or mobile offshore drilling units which will only operate through the summer. The estimation of extreme value models which accommodate directional and seasonal variability is therefore of considerable interest.

There is a large literature on applied extreme value analysis relevant to ocean engineering. Threshold methods in extreme value analysis are reviewed by Ref. [1]. Tancredi et al. [2] considered accounting for threshold uncertainty in extreme value analysis. Wadsworth and Tawn [3] presented likelihood-based procedures for threshold diagnostics and uncertainty. Thompson et al. [4] proposed automatic threshold selection for extreme value analysis. Thompson et al. [5] reported Bayesian nonparametric regression using splines. Muraleedharan et al. [6] and Cai and Reeve [7] modeled significant wave height distributions with quantile functions for estimation of extreme wave heights. Scotto and Guedes-Soares [8,9] discussed the long-term prediction of significant wave height. Methods for analysis of time-series extremes are reviewed by Chavez-Demoulin and Davison [10]. Ferro and Segers [11] and Fawcett and Walshaw [12] discussed modeling of clustered extremes. Mendez et al. [13] considered long-term variability of extreme significant wave height using a time-dependent POT model. Ruggiero et al. [14] reported increasing wave heights and extreme value projections for the U.S. Pacific Northwest. Calderon-Vega et al. [15] modeled seasonal variation of extremes in the Gulf of Mexico using a time-dependent GEV model. Mendez et al. [16] considered the seasonality and duration in extreme value distributions of significant wave height. Mackay et al. [17]

Contributed by the Ocean, Offshore, and Arctic Engineering Division of ASME for publication in the Journal of Offshore Mechanics and Arctic Engineering. Manuscript received April 23, 2014; final manuscript received January 15, 2015; published online February 10, 2015. Assoc. Editor: Arvid Naess.

discussed discrete seasonal and directional models for the estimation of extreme wave conditions. Eastoe and Tawn [18] modeled nonstationary extremes with application to surface level ozone. Chavez-Demoulin and Davison [19] provided a nice introduction to modeling nonstationary extremes using splines, and Davison et al. [20] provided a good introduction to spatial extremes. Jonathan and Ewans [21] overviewed extreme value analysis from a met-ocean perspective.

Extreme value models for storm severity are generally estimated using storm peak significant wave height H_S^{sp} (see, for example, Ref. [21]), so that each independent storm event is represented just once in the sample for statistical modeling. Simulation under this model allows estimation of the distribution of maximum storm peak significant wave height in any return period of interest. To account for within-storm (henceforth intrastorm) evolution of significant wave height H_S (as opposed to H_S^{sp}), simulation of H_S for all storm sea-states is necessary.

Capturing covariate effects of extreme sea-states is important when developing design criteria. In previous works (see, for example, Refs. [22,23]). it has been shown that omnidirectional design criteria derived from a nonstationary model which adequately incorporates covariate effects can be materially different from a stationary model which ignores those effects (see, for example, Ref. [24]). Similar effects have been demonstrated for seasonal covariates (see, for example, Refs. [24,25]). Randell et al. [26] and Jonathan et al. [27] reported a spatiodirectional model for storm peak significant wave height, H_S^{sp} in the Gulf of Mexico, in which the characteristics of extreme values vary with storm direction and location.

A nonstationarity extreme value model is generally superior to the alternative "partitioning" method sometimes used within the ocean engineering community. In the partitioning method, the sample of storm peak significant wave heights H_S^{sp} is partitioned into subsets corresponding to approximately constant values of covariates; independent extreme value analysis is then performed on each subset. For example, in the current application we might choose to partition the sample into directional octants and seasonal quarters, and then estimate (stationary) extreme value models for each of the 32 ($= 8 \times 4$) subsets. There are two main reasons for favoring a nonstationarity model over the partitioning method. First, the partitioning approach incurs a loss in statistical efficiency of estimation, since parameter estimates for subsets with similar covariate values are estimated independently of one another, even though physical insight would require parameter estimates to be similar. In the nonstationary model, we *require* that parameter estimates corresponding to similar values of covariates be similar, and optimize the degree of similarity using cross-validation. For this reason, parameter uncertainty from the nonstationary model is generally smaller than from the partitioning approach. Second, the partitioning approach assumes that, within each subset, the subsample for extreme value modeling is homogeneous with respect to covariates. In general it is difficult to estimate what effect this assumption might have on parameter and return value estimates (especially when large intervals of values of covariates are combined into a subset). In the nonstationary model, we avoid the need to make this assumption completely.

Whilst the extreme significant wave height is an important parameter in the process of deriving extreme loads on an offshore structure, the largest load experienced by a structure will usually be due to the effect of a single wave rather than to the whole sea-state. In fact, for offshore platforms the most significant characteristics are: (a) the return period maximum wave height and its associated wave period, from which extreme kinematics can be derived (in conjunction with a wave theory such as Stokes fifth-order or NewWave [28,29]), and (b) the return period total extreme water level, namely the sum of tide, surge, and wave crest, used to determine whether there is wave-in-deck loading, typically at the 10,000-year level. Estimation of return values for maximum individual wave H_{max} and maximum crest C_{max} per sea-state requires the consideration of their intrastorm probability distributions for wave height H and crest elevation C [30,31], respectively, given sea-state characteristics including H_S.

The cumulative distribution function (CDF) for the maximum wave height H_{max} in a sea-state of n_s waves with significant wave height $H_S = h_s$ is taken (see, for example, Ref. [32]) to be given by

$$P(H_{max} \le h_{max} | H_S = h_s, M = n_s) = \left(1 - \exp\left(-\frac{1}{\beta}\left(\frac{h_{max}}{h_s/4}\right)^{\alpha}\right)\right)^{n_s}$$

with $\alpha = 2.13$ and $\beta = 8.42$. The number of waves n_s in a particular sea-state is estimated by dividing the length of the sea-state (in seconds) by its zero-crossing period, T_Z.

The objective of the current work is to estimate 100-year design values for significant wave height H_S and maximum wave height H_{max} based on a sample of oceanographic time series for a North Sea location (introduced in Sec. 2). There are two key components of the modeling procedure, the first being the estimation of a directional–seasonal extreme value model for storm peak significant wave height H_S^{sp} (discussed in Sec. 3). The second component is the simulation of realizations of H_S^{sp} (for the storm peak sea-state) under the model, and thereby simulation of H_S and H_{max} for all storm sea-states (all outlined in Sec. 4). Simulation of H_S for all sea-states is achieved using so-called *intrastorm trajectories* isolated from the original time series (see Sec. 2 and the Appendix). Simulation of H_{max} requires the incorporation of the intrastorm probability distributions for H_{max} given H_S. Diagnostic plots for validation of the estimated model are presented in Sec. 5. Current and future developments are outlined in the discussion (Sec. 6).

2 Data

The application data consist of hindcast time series (from Ref. [33]) for significant wave height H_S, (dominant) wave direction θ, season ϕ (defined as day of the year, for a standardized year consisting of 360 days), mean zero up-crossing period T_Z (required for sampling from the distribution of maximum wave height H_{max} for a given sea-state, as outlined above), and period T_{01} (required for the Forristall crest height distribution, see below) for 3 hr sea-states for the period September 1957 to December 2012 at a northern North Sea location. Aarnes et al. [34] and Breivik et al. [35] have studied extreme value characteristics of storm severities from the hindcast.

Storm peak characteristics and intrastorm trajectories are isolated from these time series using the procedure described in Ref. [23]. Briefly, contiguous intervals of H_S above a low *peak-picking* threshold are identified, each interval corresponding to a storm event. The peak-picking threshold corresponds to a directional quantile of H_S with specified nonexceedance probability, estimated using quantile regression. The maximum of significant wave height during the interval is taken as the storm peak significant wave height for the storm. The value of other variables at the time of the storm peak significant wave height is referred to as storm peak values of those variables. Consecutive storms within 24 hrs of one another are combined. The resulting storm peak sample consists of 2761 values of H_S^{sp}. With direction from which a storm travels expressed in degrees clockwise with respect to north, Fig. 1 consists of scatter plots of H_S^{sp} versus storm peak direction θ^{sp} and storm peak season ϕ^{sp}. Figure 2 shows empirical quantiles of H_S^{sp} by θ^{sp} and θ^{sp}.

Figure 2 shows that storm intervals and storm peak values are identified for most directions and seasons using the peak-picking procedure. The effect of fetch variability with direction on storm peak values is clear from the upper panel of Fig. 1. For storms emanating from the north-east (i.e., from approximately 45 deg), there is only one occurrence of an event appreciably above 4*m* regardless of season. Further inspection of Fig. 2 shows that, even during winter months, storm severities from [0,90) are low

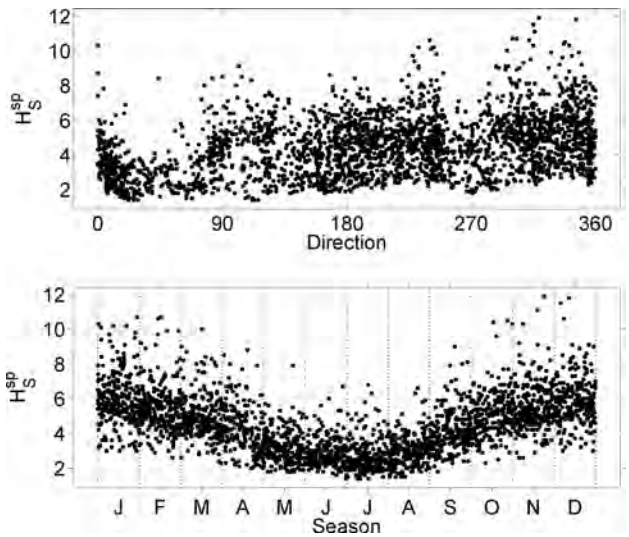

Fig. 1 Storm peak significant wave height H_S^{sp} on storm direction θ^{sp} (upper panel) and storm season ϕ^{sp} (lower panel)

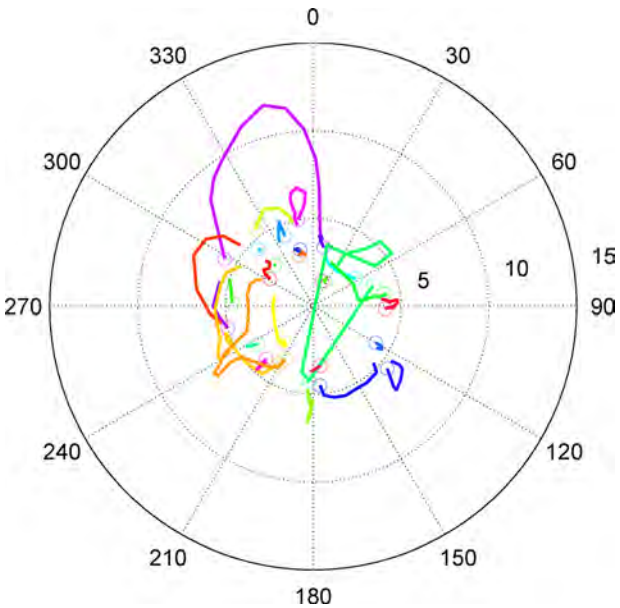

Fig. 3 Storm trajectories of significant wave height, H_S, on wave direction θ for 30 randomly chosen storm events (in different colors (or grayscales)). A circle marks the start of each intrastorm trajectory.

compared with events from other directions. These storms are very unlikely to influence estimates for omnidirectional or omniseasonal return values, but they will influence estimation of directional and seasonal return values for the directions and seasons concerned.

Corresponding to each storm and storm peak quadruplet H_S^{sp}, θ^{sp}, ϕ^{sp}, and T_Z^{sp}, the within-storm time series of H_S, θ, ϕ, and T_Z are together referred to as the *intrastorm trajectory* for the storm. Intrastorm trajectories are essential for estimation of design values for intrastorm characteristics H_S and H_{max} in Sec. 4. Figure 3 shows intrastorm trajectories of significant wave height, H_S, on wave direction θ for 30 randomly chosen storm events (in

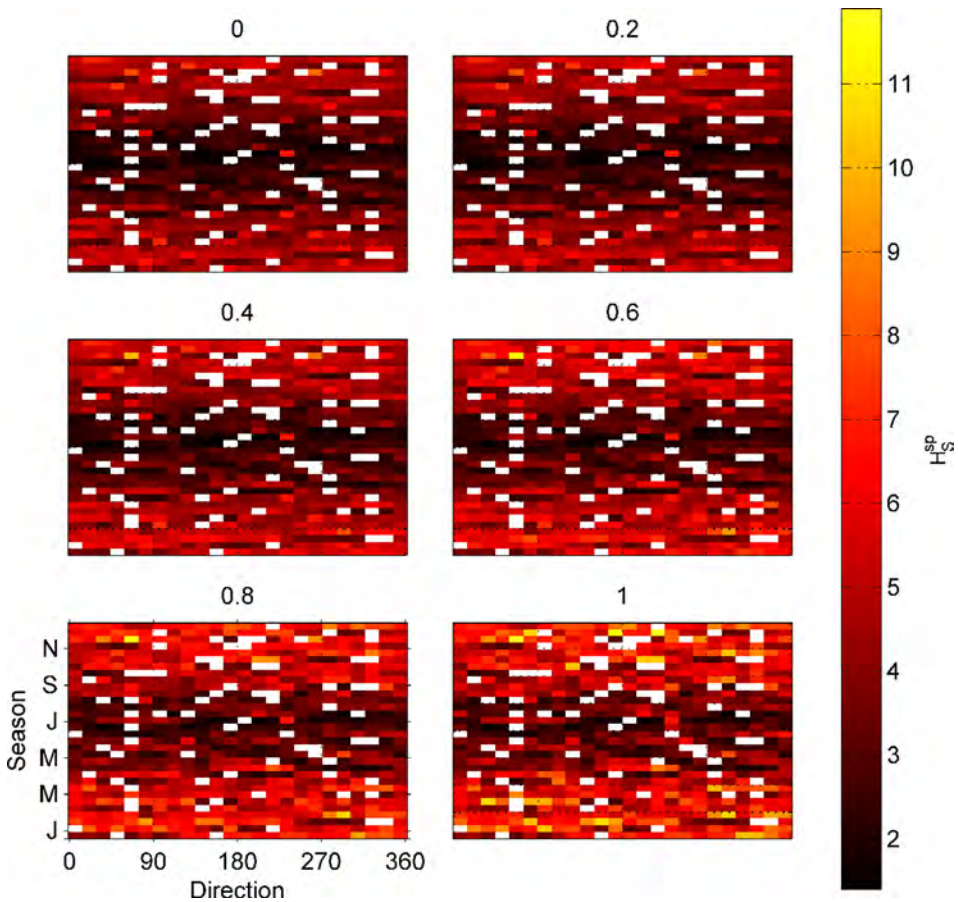

Fig. 2 Empirical quantiles of storm peak significant wave height, H_S^{sp} by storm direction, θ^{sp}, and storm season, ϕ^{sp}. Panel titles indicate quantile nonexceedance probability. Empty bins are colored white.

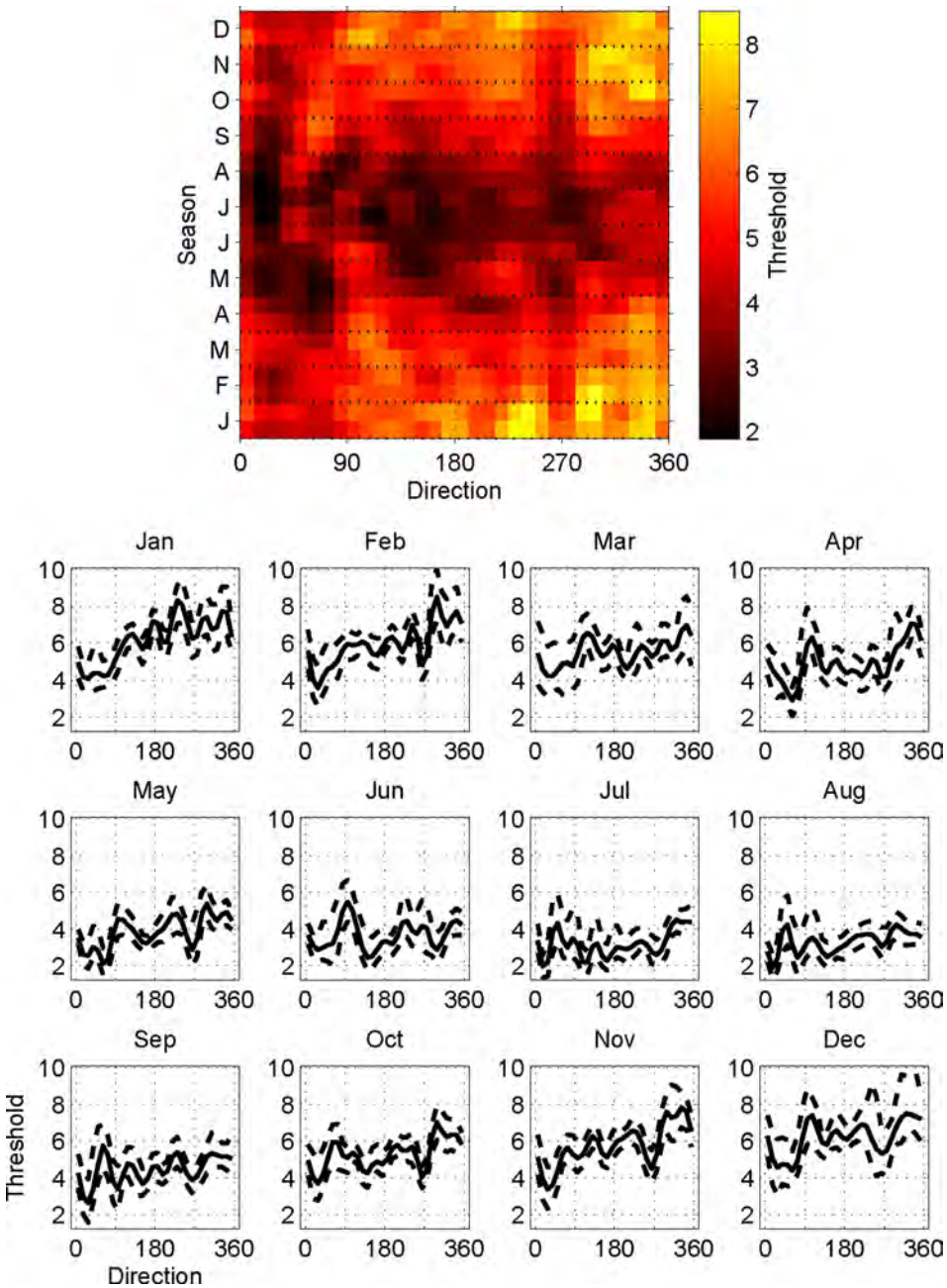

Fig. 4 Directional–seasonal parameter plot for extreme value threshold, ψ, corresponding to nonexceedance probability 0.5 of H_S^{sp}. The upper panel shows the bootstrap median threshold on storm peak direction, θ^{sp}, and storm peak season, ϕ^{sp}. The lower panels show 12 monthly directional thresholds in terms of bootstrap median (solid) and 95% bootstrap uncertainty band (dashed).

different colors (or grayscales)). The variability in storm length and storm directions covered is clear.

3 Extreme Value Model

We seek to estimate a nonstationary extreme value model for storm peak significant wave height H_S^{sp}, the parameters of which vary smoothly with respect to storm peak direction θ_{sp} and season ϕ_{sp}.

3.1 Model Components. Following Ref. [26], for a sample $\{\dot{z}_i\}_{i=1}^{\dot{n}}$ of $\dot{n}$ storm peak significant wave heights observed with storm peak directions $\{\dot{\theta}_i\}_{i=1}^{\dot{n}}$ and storm peak seasons $\{\dot{\phi}_i\}_{i=1}^{\dot{n}}$ (henceforth together referred to as covariates), we proceed using the peaks over threshold approach as follows.

3.1.1 Threshold. We first estimate a threshold function ψ above which observations $\dot{z}$ are assumed to be extreme. The threshold varies smoothly as a function of covariates $(\psi \triangleq \psi(\theta, \phi))$ and is estimated using quantile regression. We retain the set of n threshold exceedances $\{z_i\}_{i=1}^{n}$ observed with storm peak directions $\{\theta_i\}_{i=1}^{n}$ and storm peak seasons $\{\phi_i\}_{i=1}^{n}$ for further modeling.

3.1.2 Rate of Occurrence of Threshold Exceedance. We next estimate the rate of occurrence ρ of threshold exceedance using a Poisson process model with Poisson rate $\rho(\triangleq \rho(\theta, \phi))$.

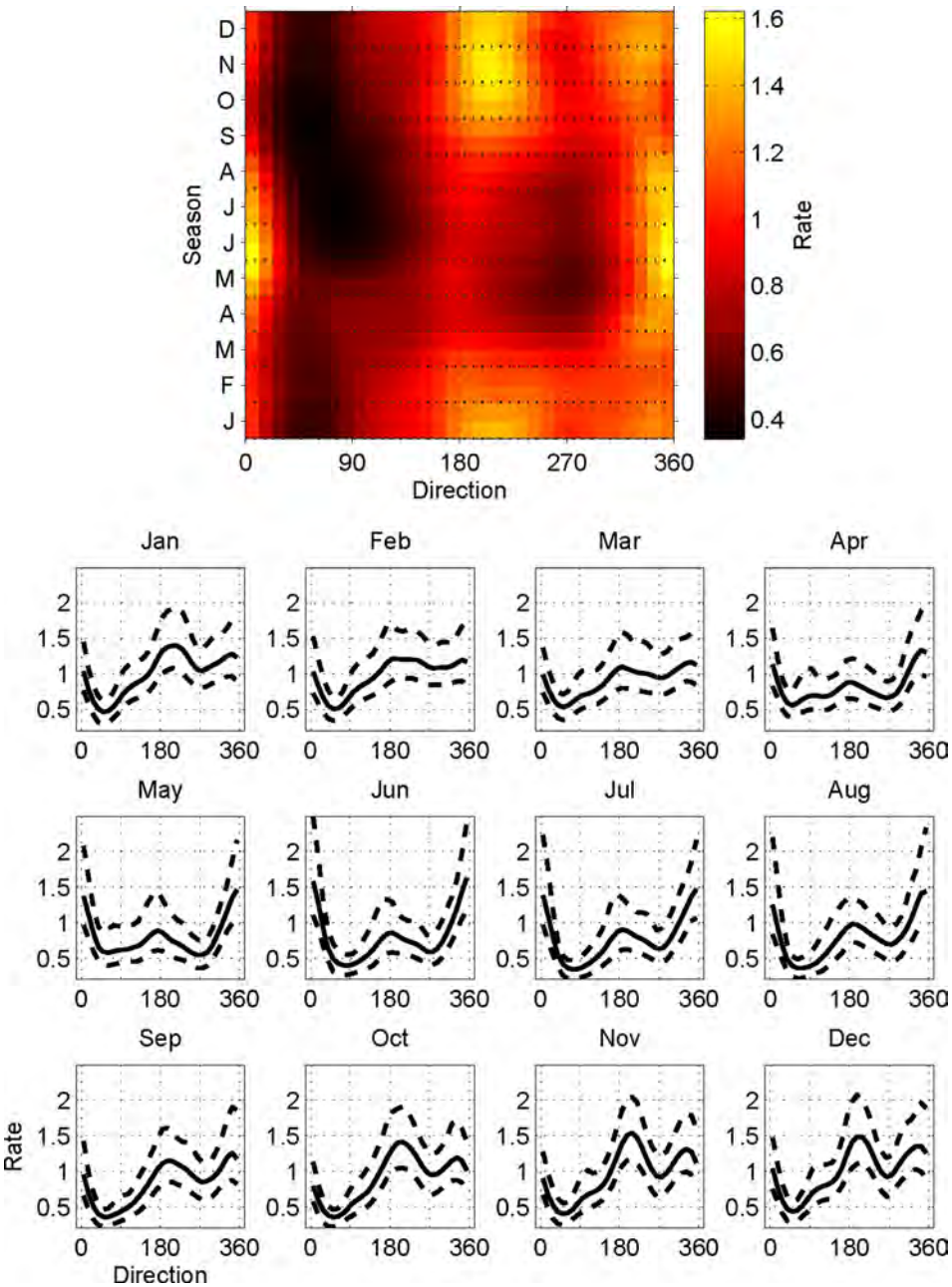

Fig. 5 Directional–seasonal parameter plot for rate of threshold exceedance, $\rho\times10^4$, of H_S^{sp}. The upper panel shows the bootstrap median rate on θ^{sp} and ϕ^{sp}. The lower panels show 12 monthly directional rates in terms of bootstrap median (solid) and 95% bootstrap uncertainty band (dashed). Unit of rate ρ is number of occurrences per annum per directional–seasonal covariate bin.

3.1.3 Size of Occurrence of Threshold Exceedance. We estimate the size of occurrence of threshold exceedance using a GP model. The GP shape and scale parameters ξ and σ are also assumed to vary smoothly as functions of covariates.

This approach to extreme value modeling follows that of Ref. [19] and is equivalent to direct estimation of a nonhomogeneous Poisson point process model (see, for example, Ref. [21,36]).

3.2 Parameter Estimation. For quantile regression, we seek a smooth function ψ of covariates corresponding to nonexceedance probability τ of storm peak H_S for any combination of θ, ϕ. We estimate ψ by minimizing the quantile regression lack of fit criterion

$$\ell_\psi = \left\{ \tau \sum_{i,r_i \geq 0}^{n} |r_i| + (1-\tau) \sum_{i,r_i<0}^{n} |r_i| \right\}$$

for residuals $r_i = z_i - \psi(\theta_i, \phi_i; \tau)$. We regulate the smoothness of the quantile function by penalizing lack of fit for parameter roughness R_ψ (with respect to all covariates), by minimizing the penalized criterion

$$\ell_\psi^* = \ell_\psi + \lambda_\psi R_\psi$$

where the value of roughness coefficient λ_ψ is selected using cross-validation to provide good predictive performance.

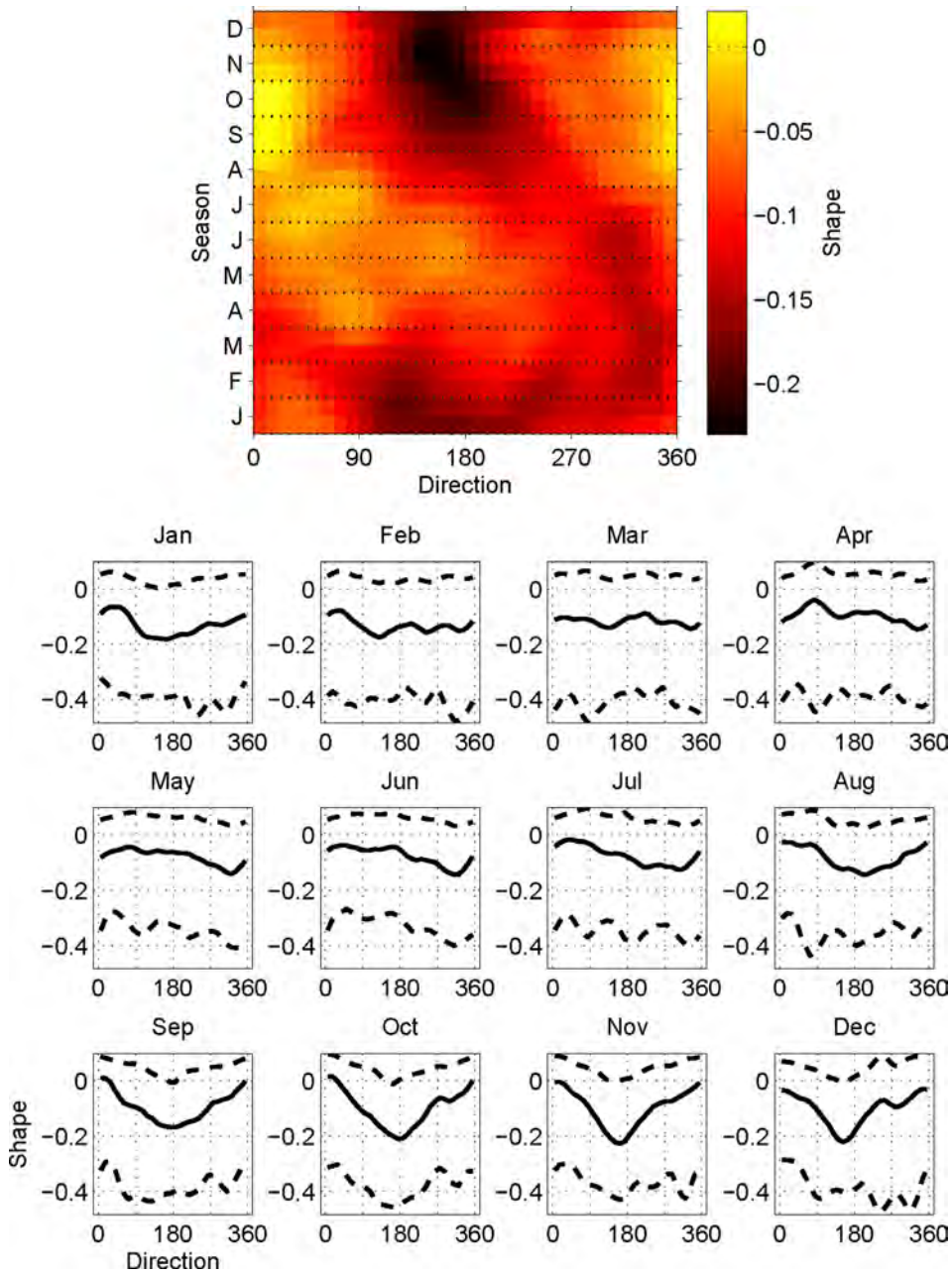

Fig. 6 Directional–seasonal parameter plot for GP shape, ξ. The upper panel shows the bootstrap median shape on θ^{sp} and ϕ^{sp}. The lower panels show 12 monthly directional shapes in terms of bootstrap median (solid) and 95% bootstrap uncertainty band (dashed).

For Poisson modeling, we use penalized likelihood estimation. The rate ρ of threshold exceedance is estimated by minimizing the roughness-penalized (negative log) likelihood

$$\ell_\rho^* = \ell_\rho + \lambda_\rho R_\rho$$

where R_ρ is parameter roughness with respect to all covariates, λ_ρ is again evaluated using cross-validation, and Poisson (negative log) likelihood is given by

$$\ell_\rho = -\sum_{i=1}^{n} \log\rho(\theta_i, \phi_i) + \int \rho(\theta, \phi) d\theta dx dy$$

The GP model of size of threshold exceedance is estimated in a similar manner by minimizing the roughness penalized (negative log) GP likelihood

$$\ell_{\xi,\sigma}^* = \ell_{\xi,\sigma} + \lambda_\xi R_\xi + \lambda_\sigma R_\sigma$$

where R_ξ and R_σ are parameter roughness with respect to all covariates, λ_ξ and λ_σ are evaluated using cross-validation, and GP (negative log) likelihood is given by

$$\ell_{\xi,\sigma} = \sum_{i=1}^{n} \log\sigma_i + \left(\frac{1}{\xi_i} + 1\right) \log\left(1 + \frac{\xi_i}{\sigma_i}(z_i - \psi_i)\right)$$

where $\psi_i = \psi(\theta_i, \phi_i)$, $\xi_i = \xi(\theta_i, \phi_i)$, and $\sigma_i = \sigma(\theta_i, \phi_i)$, and a similar expression is used when $\xi_i = 0$ (see, Ref. [21]). In practice, we set $\lambda_\xi = \kappa\lambda_\sigma$ for prespecified constant κ, so that only one cross-validation loop is necessary. The value of κ is estimated by inspection of the relative smoothness of ξ and σ with respect to covariates.

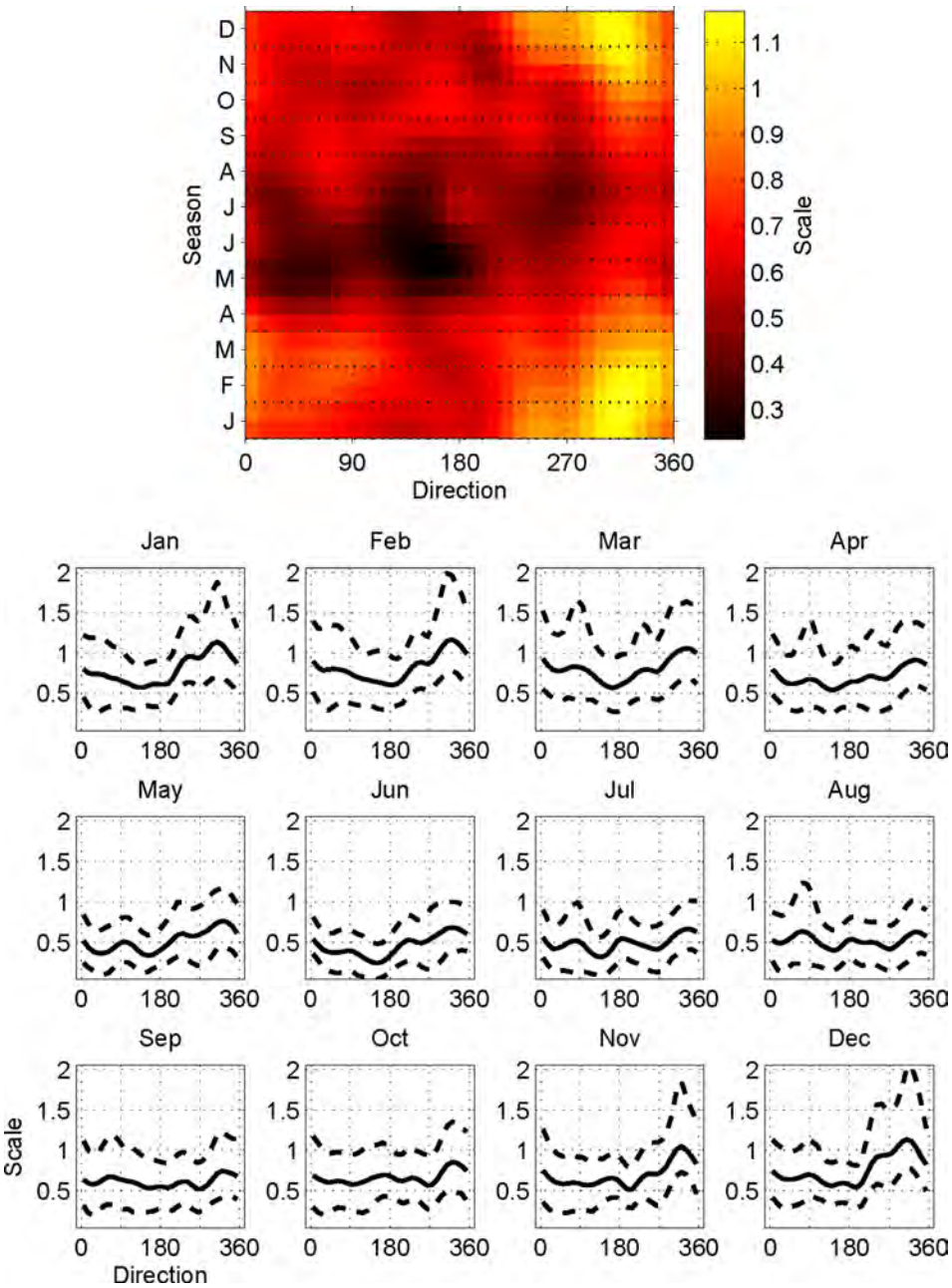

Fig. 7 Directional–seasonal parameter plot for GP scale, σ. The upper panel shows the bootstrap median scale on θ^{sp} and ϕ^{sp}. The lower panels show 12 monthly directional scales in terms of bootstrap median (solid) and 95% bootstrap uncertainty band (dashed).

3.3 Parameter Smoothness. Physical considerations suggest that we should expect the model parameters ψ, ρ, ξ, and σ to vary smoothly with respect to covariates θ, ϕ. For estimation, this can be achieved by expressing each parameter in terms of an appropriate basis for the domain D of covariates, where $D = D_\theta \times D_\phi$. $D_\theta = D_\phi = [0, 360)$ are the (marginal) domains of storm peak direction and season, respectively, under consideration. We calculate a periodic marginal B-spline basis matrix B_θ for an index set of 32 directional knots, and a periodic marginal B-spline basis matrix B_ϕ for an index set of 24 seasonal bins yielding a total of $m(= 32 \times 24)$ combinations of covariate values. Then, we define a basis matrix for the two-dimensional domain D using Kronecker products of the marginal basis matrices. Thus

$$B = B_\phi \otimes B_\theta$$

provides a $(m \times p)$ basis matrix (where $m = 32 \times 24$ and $p = p_\theta p_\phi$) for modeling each of ψ, ρ, ξ, and σ, any of which can be expressed in the form $B\beta$ for some $(p \times 1)$ vector of basis coefficients. Model estimation therefore reduces to estimating appropriate sets of basis coefficients for each of ψ, ρ, ξ, and σ.

The roughness R of any function can be easily evaluated on the index set (at which $\eta = B\beta$). Following the approach of Eilers and Marx (see, for example, Ref. [37]), we define roughness using

$$R = \beta' P \beta$$

where P can be easily evaluated for the marginal and three-dimensional domains. The form of P is motivated by taking differences of neighboring values of β, thereby penalizing lack of local

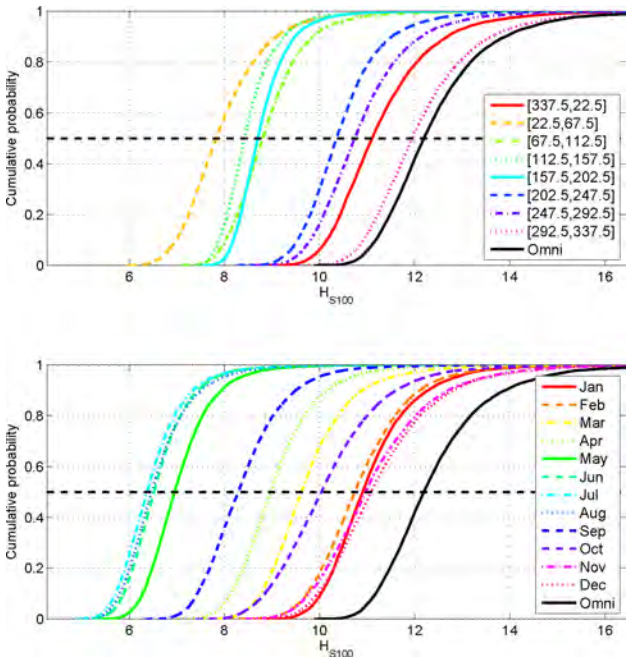

Fig. 8 CDFs for 100-year storm peak significant wave height, H_{S100} from simulation under the directional–seasonal model, incorporating uncertainty in parameter estimation using bootstrap resampling. Upper panel shows CDFs for directional octants and lower panel for months of year. The common omnidirectional omniseasonal CDF is shown in both panels (in black).

smoothness. The values of p_θ and p_ϕ are functions of the number of spline knots for each marginal domain and also depend on whether spline bases are specified as periodic (which is the case for both marginal bases in this application).

3.4 Uncertainty Quantification. Bootstrap resampling is used for uncertainty quantification. 95% bootstrap uncertainty bands are estimated by repeating the full extreme value analysis for 1000 resamples of the original storm peak sample. In particular, estimation of optimal roughness penalties is performed independently for each bootstrap resample, so that uncertainty bands also reflect variability in these choices. It was also confirmed that 1000 resamples were sufficient to ensure stability of bootstrap confidence intervals.

3.5 Estimated Parameters. Figure 4 shows plots for extreme value threshold ψ, corresponding to nonexceedance probability 0.5 of H_S^{sp}. The upper panel shows the bootstrap median threshold on storm peak direction θ^{sp} and storm peak season ϕ^{sp}. The lower panels show 12 monthly directional thresholds in terms of bootstrap median (solid) and 95% bootstrap uncertainty band (dashed). From inspection of the upper image, it is clear that summer periods are relatively calm, as are storm events from directions in $[0, 90)$. Figure 5 shows plots for rate of threshold exceedance ρ of H_S^{sp}. The upper panel shows the bootstrap median rate on θ^{sp} and ϕ^{sp}. The lower panels show 12 monthly directional rates in terms of bootstrap median (solid) and 95% bootstrap uncertainty band (dashed). The rate of occurrence of threshold exceedances is largest for winter storms from either around 180 deg or 360 deg.

Figure 6 shows plots for GP shape ξ. The upper panel shows the bootstrap median shape on θ^{sp} and ϕ^{sp}. The lower panels show 12 monthly directional shapes in terms of bootstrap median (solid) and 95% bootstrap uncertainty band (dashed). The corresponding plots for GP scale σ are given in Fig. 7. ξ shows greatest directional variability in the months of October–December, but the uncertainty in the estimates of ξ is relatively large (so that a constant model would suffice for this application). The estimates of σ show greater variation; largest values are observed for winter storms emanating from directions in [270,360).

4 Estimation of Return Values

Return values corresponding to some return period P of interest are estimated by simulation under the model developed in Sec. 3. The procedure is as follows, for each of a large number N of realizations of storms:

(1) Select a bootstrap resample and the corresponding estimated directional–seasonal extreme value model for storm peak significant wave height.
(2) For each directional–seasonal covariate bin, estimate the number of storm peak realizations to be drawn at random using the estimated directional–seasonal rate of threshold exceedance, ρ, for that bin, scaled to return period, P. If T is the period of the original sample, the scaled rate is $\rho * P/T$). Then, for each storm peak realization:
   (a) Draw a pair of values for storm peak direction θ^{sp*} and storm peak season ϕ^{sp*} at random from the volume corresponding to the covariate bin.
   (b) Draw a value of storm peak significant wave height H_S^{sp*} corresponding to θ^{sp*} and ϕ^{sp*}, at random from the corresponding GP model.
   (c) Draw an intrastorm trajectory corresponding to the triplet $(H_S^{sp*}, \theta^{sp*}, H_S^{sp*}$, and $\phi^{sp*})$, using the procedure described in the Appendix.
   (d) For each sea-state in the intrastorm trajectory, use closed-form distributions for maximum wave height H_{max} to sample values H_{max}^*.
(3) Accumulate maximum values for storm peak (H_S^{sp*}) and intrastorm H_{max}^* variables per directional–seasonal covariate bin.

Empirical CDFs for storm peak and intrastorm maxima are then trivially estimated by sorting the values for each variable for arbitrary combinations of covariate bins. In this way, for example, CDFs for directional return values each month of the year or seasonal return values for directional octants can be estimated. By retaining only maxima over all covariate bins, omnidirectional omniseasonal is obtained. Importantly, since realizations based on models from different bootstrap resamples of the original sample are used, the resulting CDFs incorporate both the (aleatory) inherent randomness of return values and the extra (epistemic) uncertainty introduced by model parameter estimation from a sample of data. Figure 8 shows CDFs for 100-year storm peak significant wave height H_{S100} from simulation under the directional–seasonal model, incorporating uncertainty in parameter estimation using bootstrap resampling as explained above. Upper panel shows CDFs for directional octants and lower panel for months of year. The common omnidirectional omniseasonal CDF is shown in both panels (in black). It is clear that the severest storms come from the north-west in winter months. The median omnidirectional omniseasonal 100-year storm peak value is approximately 12.2 m. Figure 9 shows return value plots for 100-year significant wave height H_{S100}. The upper panel shows omniseasonal return values on wave direction θ, in terms of directional octant median (solid black), most-probable (dot-dashed black), 2.5‰ and 97.5‰ (both dashed black), and the corresponding omnidirectional omniseasonal estimates (in red (or gray), common to Fig. 10). The lower panels show 12 monthly directional octant return values (in black) in terms of median (solid), most-probable (dot-dashed), and 2.5‰ and 97.5‰ (both dashed). The corresponding omnidirectional estimates are also shown (in red (or gray)). Figure 10 also shows return value plots for H_{S100}. But now the upper panel shows omnidirectional return values on wave season ϕ, in terms of monthly

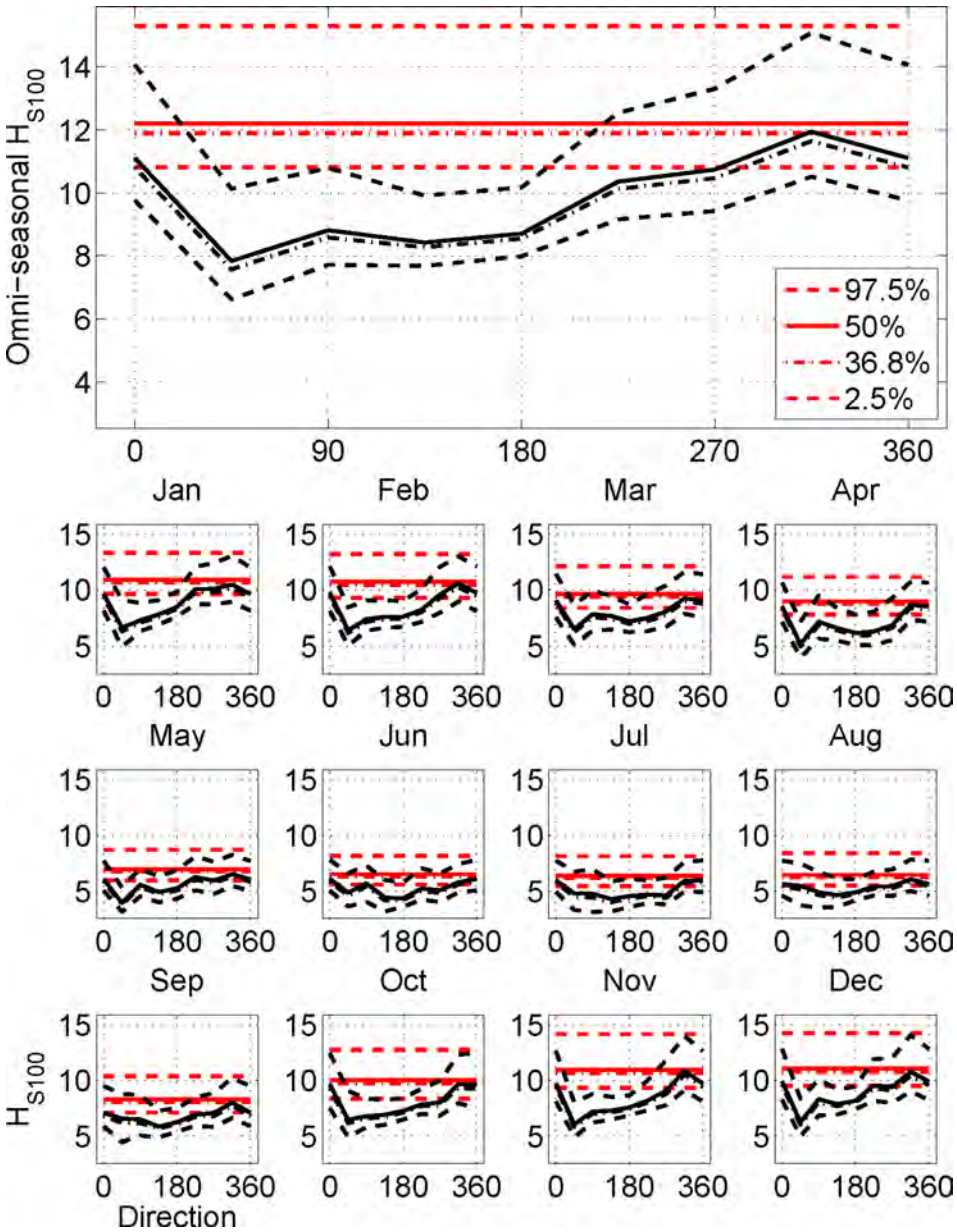

Fig. 9 Directional–seasonal return value plot for 100-year significant wave height, H_{S100}. The upper panel shows omniseasonal return values on wave direction, θ, in terms of directional octant median (solid black), most-probable (dot-dashed black), 2.5 and 97.5 (both dashed black), and the corresponding omnidirectional omniseasonal estimates (in red (or gray), common to Fig. 10). The lower panels show 12 monthly directional octant return values (in black) in terms of median (solid), most-probable (dot-dashed), 2.5 and 97.5 (both dashed). The corresponding omnidirectional estimates are also shown (in red (or gray)).

median (solid black), most-probable (dot-dashed black), 2.5‰ and 97.5‰ (both dashed black), and the corresponding omnidirectional omniseasonal estimates (in red (or gray), common to Fig. 9). The lower panels show seasonal return values for directional octants in terms of median (solid), most-probable (dot-dashed), and 2.5‰ and 97.5‰ (both dashed). The corresponding omniseasonal estimates are also shown (in red (or gray)). There are obvious and statistically significant differences between return values for different directions and seasons. It is important to note that all omnidirectional and omniseasonal estimates here are calculated from the directional–seasonal model; estimating these from models which ignore directional and seasonal variation in extremes would be inappropriate.

Figure 11 shows directional–seasonal return value plots for 100-year maximum wave height $H_{\max 100}$. The upper panel shows omniseasonal return values on wave direction θ, in terms of directional octant median (solid black), most-probable (dot-dashed black), 2.5‰ and 97.5‰ (both dashed black), and the corresponding omnidirectional omniseasonal estimates (in red (or gray), common to Fig. 12). The lower panels show 12 monthly directional octant return values (in black) in terms of median (solid), most-probable (dot-dashed), and 2.5‰ and 97.5‰ (both dashed). The corresponding omnidirectional estimates are also shown (in red (or gray)). Figure 12 shows the corresponding plots for omnidirectional and directional octant extremes as a function of season. Again, there is statistically significant variation in the estimated

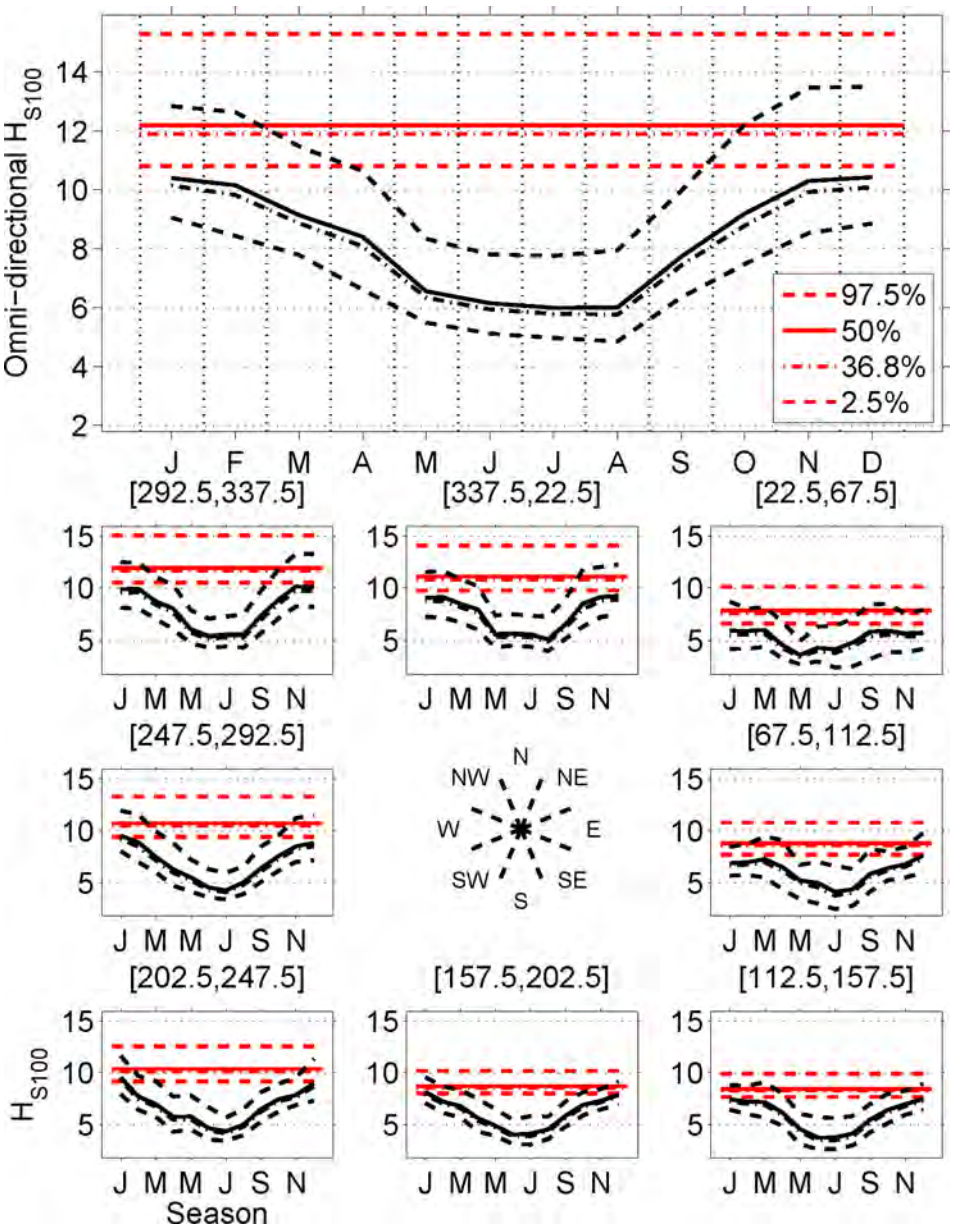

Fig. 10 Directional–seasonal return value plot for 100-year significant wave height, H_{S100}. The upper panel shows omnidirectional return values on wave season, ϕ, in terms of monthly median (solid black), most-probable (dot-dashed black), 2.5 and 97.5 (both dashed black), and the corresponding omnidirectional omniseasonal estimates (in red (or gray), common to Fig. 9). The lower panels show seasonal return values for directional octants in terms of median (solid), most-probable (dot-dashed), and 2.5 and 97.5 (both dashed). The corresponding omniseasonal estimates are also shown (in red (or gray)).

values for H_{max100}. It is unsurprising that the directional and seasonal profiles of H_{max100} closely mimic those of H_{S100}, since the intrastorm conditional distribution for H_{max} given H_S is stationary with respect to both direction and season.

5 Validation

Model diagnostics are essential to demonstrate adequate model fit. Of primary concern is that: (a) the estimated storm peak extreme value model generates directional–seasonal distributions of H_S^{sp} consistent with observed storm peak data, and that (b) the simulation procedure for estimation of return values (in Sec. 4) generates directional–seasonal distributions of H_S (for all storm sea-states) consistent with observed data. To quantify this, we use the simulation procedure to generate 1000 realizations of storms, each realization for the same period (of 55.3 years) as the original data. We then construct 95% uncertainty bands for CDFs of H_S^{sp} and H_S, partitioned by direction and season as appropriate. Then, we confirm that empirical CDFs for the actual data, for the same directional–seasonal partitions, are consistent with the simulated CDFs. Figure 13 illustrates this for H_S^{sp}. The upper panel shows the omnidirectional omniseasonal CDF for the original sample (red (or gray)), the corresponding median from simulation (solid black), together with 2.5‰ and 97.5‰ from simulation (both dashed). The lower panels compare 12 monthly CDFs in the same way. There is reasonable agreement.

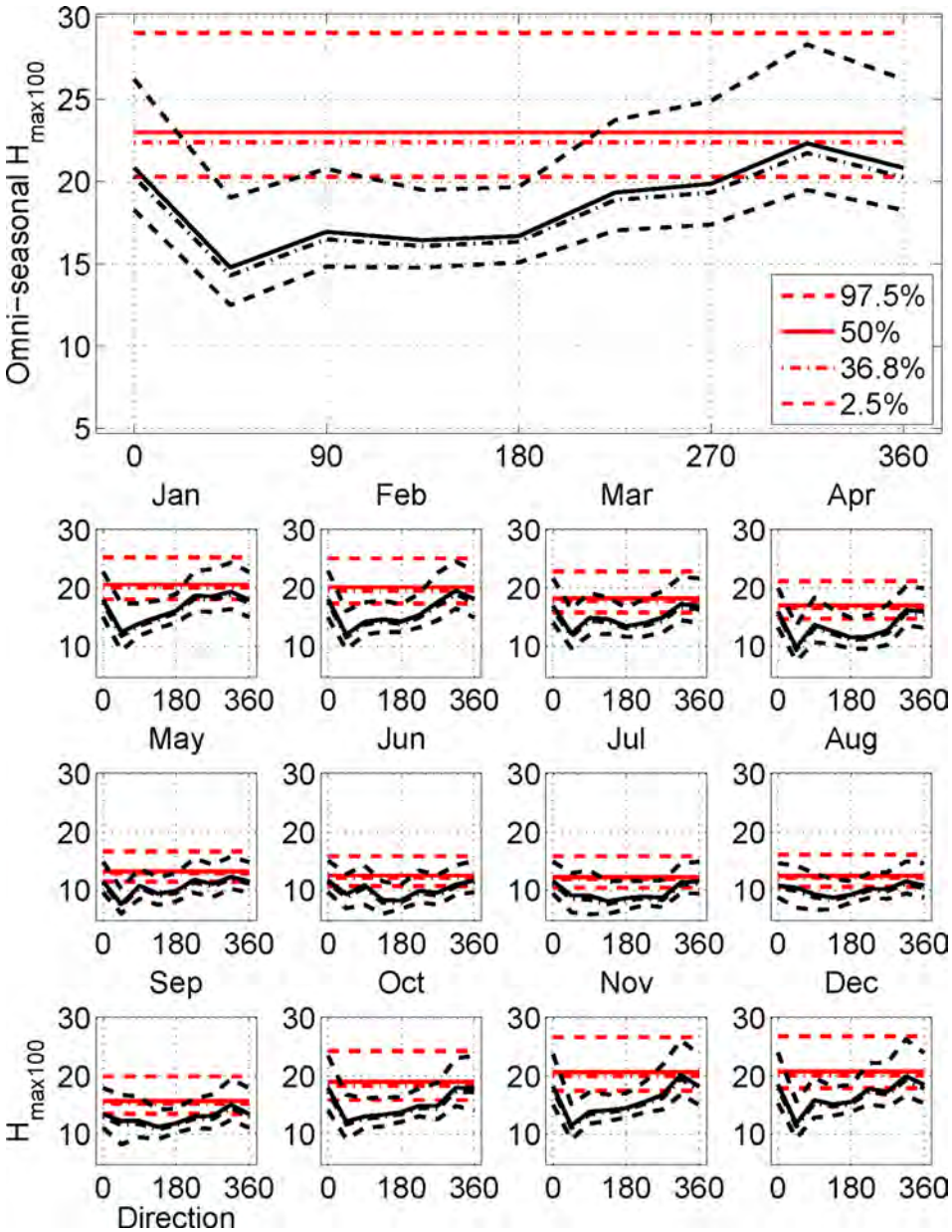

Fig. 11 Directional–seasonal return value plot for 100-year maximum wave height, H_{max100}. The upper panel shows omniseasonal return values on wave direction θ, in terms of directional octant median (solid black), most-probable (dot-dashed black), 2.5 and 97.5 (both dashed black), and the corresponding omnidirectional omniseasonal estimates (in red (or gray), common to Fig. 12). The lower panels show 12 monthly directional octant return values (in black) in terms of median (solid), most-probable (dot-dashed), and 2.5 and 97.5 (both dashed). The corresponding omnidirectional estimates are also shown (in red (or gray)).

Figure 14 illustrates the validation of directional–seasonal model for significant wave height, H_S, by comparison of CDFs for original sample with those from 1000 sample realizations under the model (incorporating intrastorm evolution of H_S) corresponding to the same time period as the original sample. The upper panel shows the omnidirectional omniseasonal CDF for the original sample (red (or gray)), the corresponding median from simulation (solid black), together with 2.5‰ and 97.5‰ from simulation (both dashed). The lower panels compare 12 monthly CDFs in the same way. Again, the agreement is good.

Plots similar to Figs. 13 and 14 showing CDFs per directional octant suggest model fit of similar quality. Since we do not have access to data for maximum wave height, we cannot apply the diagnostic procedure directly.

6 Discussion

In this work, we develop a procedure based on nonstationary extreme value analysis to estimate the distributions of storm peak significant wave height H_S^{sp} and maximum wave height H_{max} corresponding to arbitrary long return periods. The approach exploits recent advances in extreme value analysis with multidimensional covariates to characterize return value characteristics for H_S^{sp} with

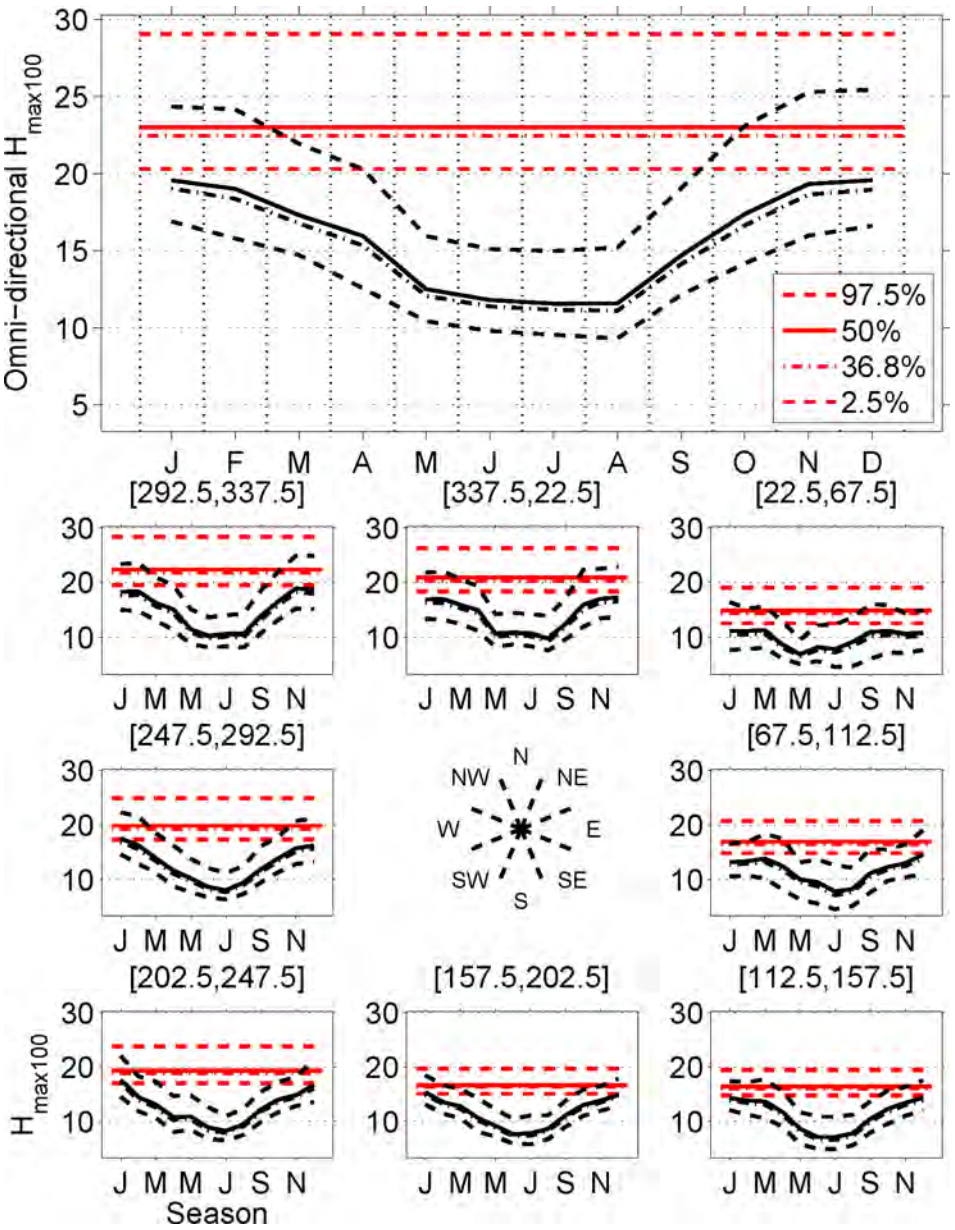

Fig. 12 Directional–seasonal return value plot for 100-year maximum wave height, H_{max100}. The upper panel shows omnidirectional return values on wave season, ϕ, in terms of monthly median (solid black), most-probable (dot-dashed black), 2.5 and 97.5 (both dashed black), and the corresponding omnidirectional omniseasonal estimates (in red (or gray), common to Fig. 11). The lower panels show seasonal return values for directional octants in terms of median (solid), most-probable (dot-dashed), and 2.5 and 97.5 (both dashed). The corresponding omniseasonal estimates are also shown (in red (or gray)).

direction and season (for the storm peak sea-state only), and simulation under the extreme value model: (a) incorporating intrastorm trajectories to estimate return value characteristics for H_S for all storm sea-states and (b) known conditional distributions for H_{max} given H_S to estimate return value characteristics for H_{max}. Diagnostic tests demonstrate that the approach performs well in application to North Sea hindcast data.

According to Ref. [38], a convolution approach should be used to correctly account for the possibility of a large wave resulting from a sea-state with relatively low severity. The simulation approach used here is similar to the numerical approach described in Ref. [39] but has a number of advantages. The current approach readily accommodates different storm characteristics from different directions, as well as seasonal variability. Furthermore, there is no need to define a single, representative storm shape; instead, actual storm histories are used reflecting natural variability within real storms.

Figures 8–12 report design values resolved into (directional) octants and (seasonal) monthly octants from simulation under the model. Design values for arbitrary directional–seasonal partitions can be estimated in the same way by simulation, in an entirely consistent fashion. For example, omnidirectional design values corresponding to the May–September period might be estimated and exploited by the designer for short-term offshore

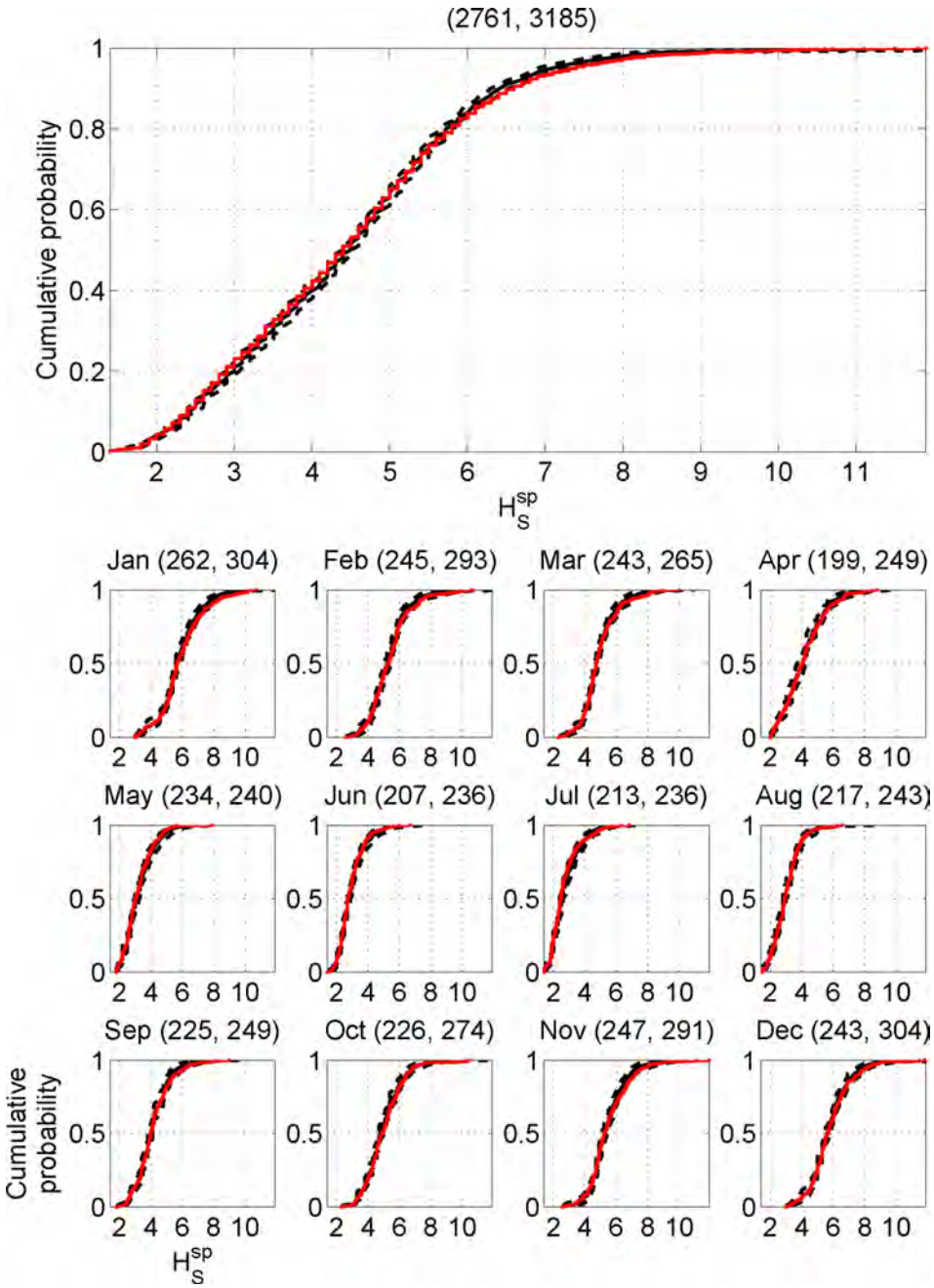

Fig. 13 Validation of directional–seasonal model for storm peak significant wave height, H_S^{sp}, by comparison of CDFs for original storm peak sample with those from 1000 sample realizations under the model corresponding to the same time period as the original sample. The upper panel shows the omnidirectional omniseasonal CDF for the original sample (red (or gray)), the corresponding median from simulation (solid black), together with 2.5 and 97.5 from simulation (both dashed). The lower panels compare 12 monthly CDFs in the same way. Titles for plots, in brackets following the month name, are the numbers of actual and simulated events in each month.

activities. In stark contrast, the lack of consistency in engineering specification of directional design criteria in particular has been the subject of some debate (see, e.g., Ref. [40]). Guidelines, such as Refs. [38,41], provide recommendations on treating directional criteria, but even when these are followed, either inconsistency remains (in the case of API), or insufficient detail is given on how to make the criteria consistent (in the case of ISO).

The method as described here has focussed on the estimation of estimation of extreme storm peak significant wave height and maximum wave height. Extension to estimation of maximum crest elevation and total extreme water level is the subject of current work and a companion publication in preparation. Since the method of incorporation of nonstationary within the extreme value modeling framework is quite general, extensions to spatial and temporal covariates (for example) are straightforward.

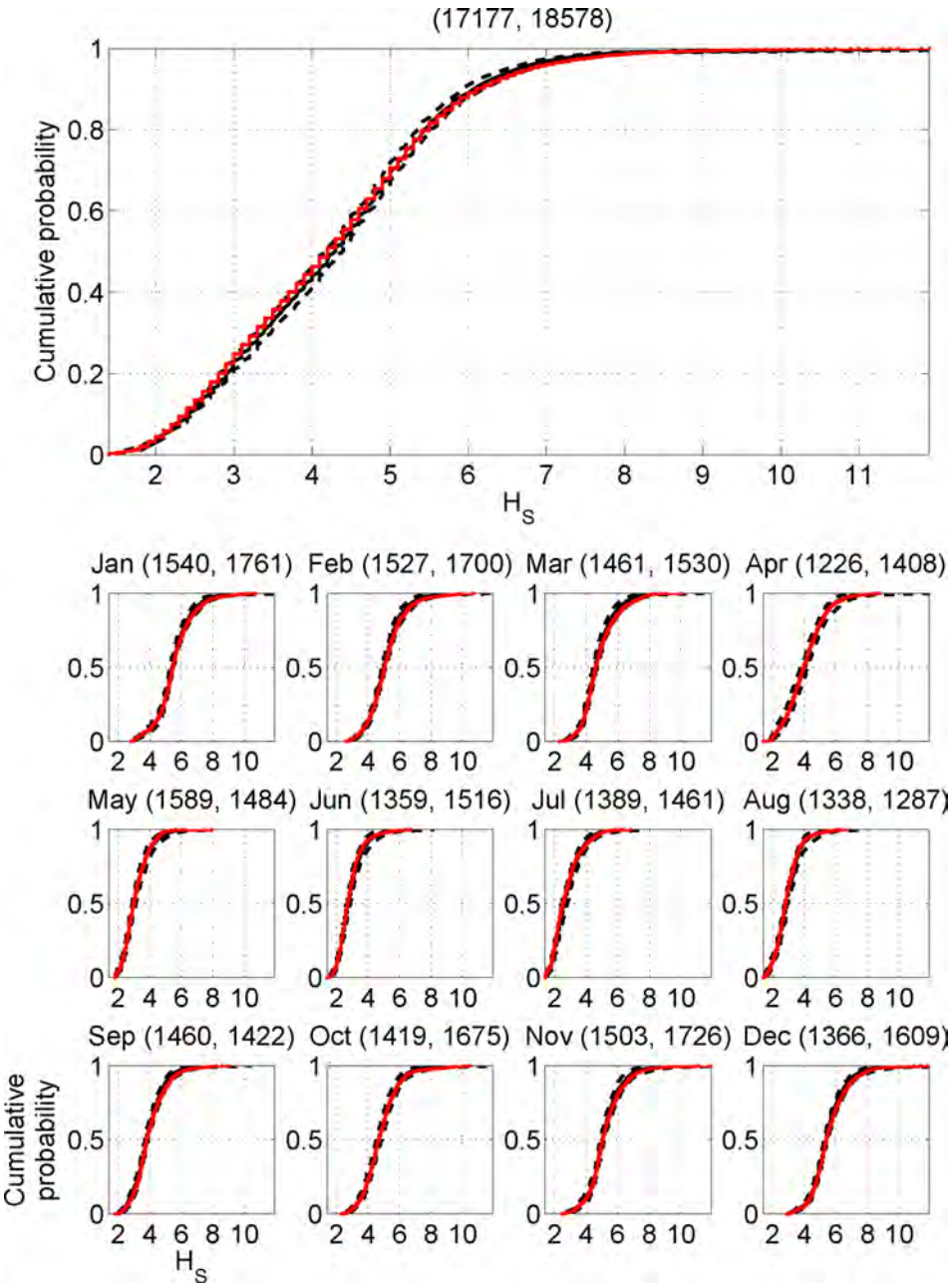

Fig. 14 Validation of directional–seasonal model for significant wave height, H_S, by comparison of CDFs for original sample with those from 1000 sample realizations under the model (incorporating intrastorm evolution of H_S) corresponding to the same time period as the original sample. The upper panel shows the omnidirectional omniseasonal CDF for the original sample (red (or gray)), the corresponding median from simulation (solid black), together with 2.5 and 97.5 from simulation (both dashed). The lower panels compare 12 monthly CDFs in the same way. Titles for plots, in brackets following the month name, are the numbers of actual and simulated events (in each month).

Acknowledgment

We acknowledge the useful discussions on computational aspects with Laks Raghupathi of Shell, Bangalore.

Appendix: Selecting Intrastorm Trajectories for Simulated Storm Events

The directional–seasonal extreme value model is estimated for storm peak significant wave height H_S^{sp}, since storm peak events provide independent events for statistical modeling. However, we require return values for significant wave height H_S from any sea-state (not just the storm peak). We also require return values for maximum wave height H_{max} and maximum crest elevation, which may or may not correspond to the storm peak sea-state. Therefore, in the simulation procedure for return value estimation described in Sec. 4, we need to generate realizations of whole intrastorm trajectories as defined in Sec. 3 not just storm peak events. We achieve this by selecting an appropriate intrastorm trajectory from the original sample, with storm peak characteristics in good agreement with those of the current storm peak realization.

Let $\{\eta_j^*\}_{j=1}^3$ represent the values of H_S^{sp*}, θ^{sp*}, and ϕ^{sp*}, respectively, for the current realization, and let $\{\eta_{ij}\}_{i=1,j=1}^{n,3}$ represent the corresponding n values for the original storm peak sample. We define the dissimilarity d_i between the ith (original) storm and the current storm peak realization as

$$d_i = \sum_{j=1}^{3} d_{ij},$$

$$d_{ij} = \frac{\eta_{ij} - \eta_j^*}{\tau_j}, \quad \text{for } c_j(\eta_{ij} - \eta_j^*) > \tau_j,$$
$$= 0 \text{ otherwise}$$

where $c_1(\bullet)$ is Euclidean distance, and $c_2(\bullet)$ and $c_3(\bullet)$ are circular distance functions defined on $[0, 360)$. The cut-off values $\{\tau_j\}_{j=1}^{3}$ indicate when the difference $c_j(\eta_{ij} - \eta_j^*)$ is sufficiently small that it can be ignored in the specification of dissimilarity. After some experimentation, values of $\tau_1 = 0.5$ (m, for H_S^{sp}), $\tau_2 = 20$ (deg, for θ^{sp}), and $\tau_3 = 45$ (deg, for ϕ^{sp}) were chosen.

The subset of original intrastorm trajectories yielding the smallest values of dissimilarity are deemed good matches to the simulated storm peak event. One of these good matching intrastorm trajectories is selected at random. The intrastorm trajectory is then adjusted: (a) so that its storm peak value is equal to H_S^{sp*} (by multiplying the H_S component of the intrastorm trajectory by an appropriate scale factor), (b) so that its storm peak direction corresponds to θ^{sp*} (by cyclic rotation of the directional component of the intrastorm trajectory), and (c) by scaling the wave period T_Z such that the sea-state steepness from the original sample is retained. The adjusted intrastorm trajectory is then allocated to the current simulated storm peak.

Using this procedure, intrastorm trajectories are allocated to simulated storm peaks, ensuring that only (adjusted) intrastorm trajectories from the original sample with similar storm peak characteristics are used, but also incorporating the inherent variability in intrastorm trajectories with respect to given storm peak characteristics.

References

[1] Scarrott, C., and MacDonald, A., 2012, "A Review of Extreme Value Threshold Estimation and Uncertainty Quantification," REVSTAT, **10**(1), pp. 33–60.

[2] Tancredi, A., Anderson, C. W., and O'Hagan, A., 2006, "Accounting for Threshold Uncertainty in Extreme Value Estimation," Extremes, **9**(2), pp. 87–106.

[3] Wadsworth, J. L., and Tawn, J. A., 2012, "Likelihood-Based Procedures for Threshold Diagnostics and Uncertainty in Extreme Value Modelling," J. R. Statist. Soc., Ser. B., **74**(3), pp. 543–567.

[4] Thompson, P., Cai, Y., Reeve, D., and Stander, J., 2009, "Automated Threshold Selection Methods for Extreme Wave Analysis," Coastal Eng., **56**(10), pp. 1013–1021.

[5] Thompson, P., Cai, Y., Moyeed, R., Reeve, D., and Stander, J., 2010, "Bayesian Nonparametric Quantile Regression Using Splines," Comput. Stat. Data Anal., **54**(4), pp. 1138–1150.

[6] Muraleedharan, G., Claudia, Lucas, Guedes Soares, C., Unnikrishnan Nair, N., and Kurup, P. G., 2012, "Modelling Significant Wave Height Distributions With Quantile Functions for Estimation of Extreme Wave Heights," Ocean Eng., **54**, pp. 119–131.

[7] Cai, Y., and Reeve, D. E., 2013, "Extreme Value Prediction Via a Quantile Function Model," Coastal Eng., **77**, pp. 91–98.

[8] Scotto, M. G., and Guedes-Soares, C., 2000, "Modeling the Long-Term Time Series of Significant Wave Height With Non-Linear Threshold Models," Coastal Eng., **40**(4), pp. 313–327.

[9] Scotto, M. G., and Guedes-Soares, C., 2007, "Bayesian Inference for Long-Term Prediction of Significant Wave Height," Coastal Eng., **54**(5), pp. 393–400.

[10] Chavez-Demoulin, V., and Davison, A. C., 2012, "Modeling Time Series Extremes," REVSTAT, **10**(1), pp. 109–133.

[11] Ferro, C. A. T., and Segers, J., 2003, "Inference for Clusters of Extreme Values," J. R. Statist. Soc., Ser. B, **65**(2), pp. 545–556.

[12] Fawcett, L., and Walshaw, D., 2007, "Improved Estimation for Temporally Clustered Extremes," Environmetrics, **18**(2), pp. 173–188.

[13] Mendez, F. J., Menendez, M., Luceno, A., and Losada, I. J., 2006, "Estimation of the Long-Term Variability of Extreme Significant Wave Height Using a Time-Dependent Pot Model," J. Geophys. Res., **111**(C7), p. C07024.

[14] Ruggiero, P., Komar, P. D., and Allan, J. C., 2010, "Increasing Wave Heights and Extreme Value Projections: The Wave Climate of the U.S. Pacific Northwest," Coastal Eng., **57**(5), pp. 539–522.

[15] Calderon-Vega, F., Vazquez-Hernandez, A. O., and Garcia-Soto, A. D., 2013, "Analysis of Extreme Waves With Seasonal Variation in the Gulf of Mexico Using a Time-Dependent GEV Model," Ocean Eng., **73**, pp. 68–82.

[16] Mendez, F. J., Menendez, M., Luceno, A., Medina, R., and Graham, N. E., 2008, "Seasonality and Duration in Extreme Value Distributions of Significant Wave Height," Ocean Eng., **35**(1), pp. 131–138.

[17] Mackay, E. B. L., Challenor, P. G., and Bahaj, A. S., 2010, "On the Use of Discrete Seasonal and Directional Models for the Estimation of Extreme Wave Conditions," Ocean Eng., **37**(5–6), pp. 425–442.

[18] Eastoe, E. F., and Tawn, J. A., 2012, "Modeling Non-Stationary Extremes With Application to Surface Level Ozone," J. R. Statist. Soc., Ser. C, **58**(1), pp. 25–45.

[19] Chavez-Demoulin, V., and Davison, A. C., 2005, "Generalized Additive Modelling of Sample Extremes," J. R. Statist. Soc., Ser. C, **54**(1), p. 207.

[20] Davison, A. C., Padoan, S. A., and Ribatet, M., 2012, "Statistical Modeling of Spatial Extremes," Stat. Sci., **27**(2), pp. 161–186.

[21] Jonathan, P., and Ewans, K. C., 2013, "Statistical Modeling of Extreme Ocean Environments With Implications for Marine Design: A Review," Ocean Eng., **62**, pp. 91–109.

[22] Jonathan, P., and Ewans, K. C., 2007, "The Effect of Directionality on Extreme Wave Design Criteria," Ocean Eng., **34**(14), pp. 1977–1994.

[23] Ewans, K. C., and Jonathan, P., 2008, "The Effect of Directionality on Northern North Sea Extreme Wave Design Criteria," ASME J. Offshore Mech. Arct. Eng., **130**(4), p. 041604.

[24] Jonathan, P., Ewans, K. C., and Forristall, G. Z., 2008, "Statistical Estimation of Extreme Ocean Environments: The Requirement for Modelling Directionality and Other Covariate Effects," Ocean Eng., **35**(11), pp. 1211–1225.

[25] Anderson, C. W., Carter, D. J. T., and Cotton, P. D., 2001, "Wave Climate Variability and Impact on Offshore Design Extremes," Report commissioned from the University of Sheffield and Satellite Observing Systems for Shell International.

[26] Randell, D., Wu, Y., Jonathan, P., and Ewans, K. C., 2013, "Modelling Covariate Effects in Extremes of Storm Severity on the Australian North West Shelf," ASME Paper No. OMAE2013-10187.

[27] Jonathan, P., Randell, D., Wu, Y., and Ewans, K., 2014, "Return Level Estimation From Non-Stationary Spatial Data Exhibiting Multidimensional Covariate Effects," Ocean Eng., **88**, pp. 520–532.

[28] Tromans, P. S., Anaturk, A., and Hagemeijer, P., 1991, "A New Model for the Kinematics of Large Ocean Waves: Application as a Design Wave," 1st International Offshore and Polar Engineering Conference (ISOPE), pp. 64–71.

[29] Jonathan, P., Taylor, P. H., and Tromans, P. S., 1994, "Storm Waves in the Northern North Sea," 7th International Conference on the Behaviour of Offshore Structures, Cambridge, MA, Vol. 2, pp. 481–494.

[30] Forristall, G. Z., 1978, "On the Statistical Distribution of Wave Heights in a Storm," J. Geophys. Res., **83**(C5), pp. 2353–2358.

[31] Forristall, G. Z., 2000, "Wave Crest Distributions: Observations and Second-Order Theory," J. Phys. Oceanogr., **30**(8), pp. 1931–1943.

[32] Prevosto, M., Krogstad, H. E., and Robin, A., 2000, "Probability Distributions for Maximum Wave and Crest Heights," Coastal Eng., **40**(4), pp. 329–360.

[33] Reistad, M., Breivik, O., Haakenstad, H., Aarnes, O. J., Furevik, B. R., and Bidlot, J.-R., 2011, "A High-Resolution Hindcast of Wind and Waves for the North Sea, the Norwegian Sea, and the Barents Sea," J. Geophys. Res., **116**, pp. 1–18.

[34] Aarnes, O. J., Breivik, O., and Reistad, M., 2012, "Wave Extremes in the Northeast Atlantic," J. Clim., **25**(5), pp. 1529–1543.

[35] Breivik, O., Aarnes, O. J., Bidlot, J.-R., Carrasco, A., and Saetra, Ø., 2013, "Wave Extremes in the North East Atlantic From Ensemble Forecasts," J. Clim., **26**(19), pp. 7525–7540.

[36] Dixon, J. M., Tawn, J. A., and Vassie, J. M., 1998, "Spatial Modeling of Extreme Sea-Levels," Environmetrics, **9**(3), pp. 283–301.

[37] Eilers, P. H. C., and Marx, B. D., 2010, "Splines, Knots and Penalties," Wiley Intersci. Rev., **2**(6), pp. 637–653.

[38] ISO19901-1, 2005, "Petroleum and Natural Gas Industries. Specific Requirements for Offshore Structures. Part 1: Metocean Design and Operating Considerations," International Standards Organization, Geneva, Switzerland.

[39] Tromans, P. S., and Vanderschuren, L., 1995, "Response Based Design Conditions in the North Sea: Application of a New Method," Offshore Technology Conference, Houston, TX, (OTC-7683).

[40] Forristall, G. Z., 2004, "On the Use of Directional Wave Criteria," J. Waterw. Port Coastal Ocean Eng., **130**(5), pp. 272–275.

[41] API, 2005, *API Recommended Practice 2A-WSD (RP 2A-WSD), Recommended Practice for Planning, Designing and Constructing Fixed Offshore Platforms: Working Stress Design*, API, Washington, DC.